Mem. S.A.It. Vol. 82, 792

**Memorie** della

# Composition and acceleration of Galactic Cosmic Rays

N. Prantzos

Institut d'Astrophysique de Paris, UMR7095 CNRS, Univ.P. & M.Curie, 98bis Bd. Arago, 75104 Paris, e-mail: prantzos@iap.fr

**Abstract.** The composition of Galactic Cosmic Rays (GCR) presents strong similarities to the standard (cosmic) composition, but also noticeable differences. The most important is the high isotopic ratio of $^{22}$Ne/$^{20}$Ne, which is ~5 times higher in GCR than in the Sun and provides key information on the GCR origin. We investigate the idea that GCR are accelerated by the forward shocks of supernova explosions, as they run through the presupernova winds of the massive stars and through the interstellar medium. We use detailed wind and core yields of rotating and non-rotating models of massive stars with mass loss, as well as simple models for the properties of the forward shock and of the circumstellar medium. We find that the observed GCR $^{22}$Ne/$^{20}$Ne ratio can be explained if GCR are accelerated only during the early Sedov phase, for shock velocities >2000 km/s. The acceleration efficiency, assumed constant during that period, is found to be of the order of $10^{-6}$-$10^{-5}$, i.e. a few particles out of a million encountered by the shock escape the SN at GCR energies.

**Key words.** Cosmic rays - acceleration of particles - abundances

## 1. Introduction

The site of the acceleration of GCR remains debatable today, despite more than five decades of theoretical and observational studies. Over the years, it has been suggested that GCR are accelerated in 1) SN remnants (either by the forward or the reverse shock or both), 2) the interstellar medium (ISM), 3) the winds of massive stars, 4) the interiors of superbubbles, excavated by the massive star winds and the subsequent SN explosions of an OB association. Each one of the proposed sites has its own advantages and shortcomings, regarding the energetics and/or the composition of accelerated matter

The most conspicuous feature of GCR source composition is undoubtely the high isotopic $^{22}$Ne/$^{20}$Ne ratio. Its value obtained from analysis of the CRIS instrument, leads to a best estimate (Binns et al. 2008) of 0.387 ± 0.007 (statistical) ± 0.022 (systematic). This is 5.3±0.3 times the value of the ($^{22}$Ne/$^{20}$Ne)$_\odot$ ratio in the solar wind. Contrary to the case of the elemental source GCR abundances, which may be affected by various physico-chemical factors (first ionization potential, condensation temperature, etc.) isotopic ratios can only be affected by nucleosynthetic processes and thus provide crucial information on the origin of cosmic ray particles.

In this work we study the $^{22}$Ne/$^{20}$Ne ratio of GCR accelerated by the forward shocks of SN explosions, as they run through the pre-

*Send offprint requests to*: N. Prantzos supernova winds of massive stars and through the interstellar medium. We consider the whole mass spectrum of massive stars (from ∼10 to 120 $M_\odot$), including stars with either small or large mass losses prior to their explosions. We consider stellar properties (masses of winds, ejecta, yields etc.) from recent models with mass loss and or without rotation (from Hirschi et al. 2005 - hereafter HMM05 - and Limongi and Chieffi 2006 - hereafter LC06 -, respectively), the former having larger $^{22}$Ne enhancements in their winds. We adopt a simplified prescription, suggested in Ptuskin and Zirakashvili (2005) and reformulated in Caprioli (2011), to describe the structure of the circumstellar medium at the time of the explosion and we consider that GCR start being accelerated in the Sedov-Taylor (ST) phase of the SN remnant (see Prantzos 2011 for a detailed description of the model and results).

## 2. Results

Fig. 1 (top and middle) displays the evolution of the velocity $\upsilon_S$ and radius $R_S$ of the forward shock and of the mass $M_S(< R_S)$ swept up by it, for the cases of a 20 and a 60 $M_\odot$ rotating star, respectively. The similarity of the curves for $\upsilon_S$, $R_S$ and $M_S(< R_S)$ for the 20 and 60 $M_\odot$ stars simply reflects the self-similarity of the ST solution. The small differences in the early ST phase are due to the difference of the ejected mass $M_{Ej}$ in the two stars.

The bottom panel of Fig. 1 displays the evolution of the $^{14}$N/$^{16}$O and $^{22}$Ne/$^{20}$Ne ratios (i.e. the ratios of the corresponding masses for each isotope), expressed in units of the corresponding solar values. The evolution of $^{22}$Ne/$^{20}$Ne is quite different in the two models. In the 20 $M_\odot$ star, no He-burning products are encountered by the shock wave and the $^{22}$Ne/$^{20}$Ne ratio has always its initial (solar) value. A high $^{22}$Ne/$^{20}$Ne ratio is initially encountered in the processed layers of the 60 $M_\odot$ star, which is progressively diluted as the shock moves outwards.

The composition curves of the bottom panel of Fig. 1 give the time (or mass) integrated composition encountered by the shock wave and, in consequence, the composition of the particles that have been accelerated *up to that time*. We assume here that *particles are accelerated to GCR energies with the same efficiency for shock velocities higher than some critical value $\upsilon_{min}$, which is the same for all stellar masses*. We determine $\upsilon_{min}$ empirically by requiring that, when averaged over a stellar Initial mass function (IMF) $\Phi(M_*)$, the ratio

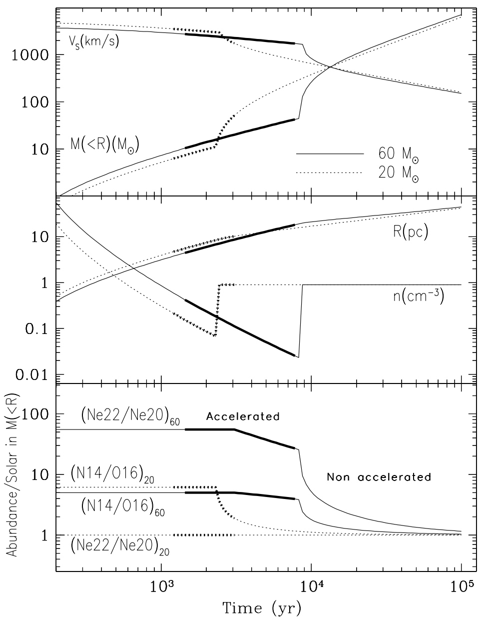


**Fig. 1.** Evolution of the SN remnants of two rotating stars of initial masses 20 $M_\odot$ (*dotted*) and 60 $M_\odot$ (*solid*), respectively. *Top*: velocity of the forward shock and swept up mass. *Middle*: Shock radius and density profile before shock arrival (see text). *Bottom:* Composition of the matter swept up up to time *t* by the shock wave, for the $^{14}$N/$^{16}$O and $^{22}$Ne/$^{20}$Ne ratios. In all panels, the *thick* portions of the curves indicate the period of efficient particle acceleration, i.e. from the beginning of the ST phase and as far as $\upsilon_s > \upsilon_{min}$. The value of $\upsilon_{min}$ (=1900 km/s for the rotating star models in the figure) is chosen so that the IMF averaged theoretical ratio of $^{22}$Ne/$^{20}$Ne matches the observed one in GCR (see Fig. 2).

$$\frac{M_{22}}{M_{20}} = \frac{\int_{10M_\odot}^{120M_\odot} dM_* m_{22}(M_*)\Phi(M_*)}{\int_{10M_\odot}^{120M_\odot} dM_* m_{20}(M_*)\Phi(M_*)} = R_{Obs}\frac{X_{22,\odot}}{X_{20,\odot}} \qquad (1)$$

where $R_{Obs}$=5.3±0.3 is the observationally determined source GCR ratio of $^{22}$Ne/$^{20}$Ne in

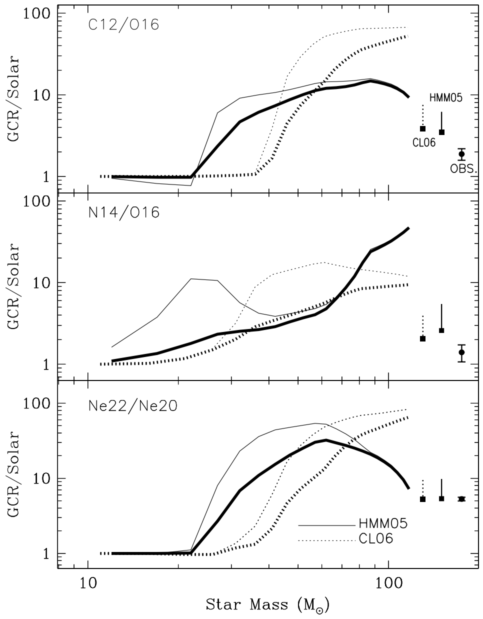


**Fig. 2.** Abundance ratios of various nuclear species in GCR source normalized to the corresponding solar ones, as a function of the initial stellar mass. In all panels, *solid curves* correspond to models of HMM05 and *dotted curves* to models of LC06. *Upper, thin curves* are for GCR accelerated at the beginning of the ST phase and *lower, thick curves* for the time-average at the end of GCR acceleration. An average over a Salpeter IMF (and accounting for the swept up mass in each case) produces the vertical segments to the right, their top point corresponding to the beginning and the bottom one to the end of the GCR acceleration phase, respectively (also indicated by *filled squares*). These results are compared to GCR source abundance ratios as derived by ACE data (points at the extreme right with error bars) in Binns et al. (2005). The most significant, unaffected by FIP, volatility etc., is the one of $^{22}$Ne/$^{20}$Ne. The end of the GCR acceleration phase is assumed to correspond to shock velocities $\upsilon_{min}$ such that the time and IMF averaged theoretical ratio (squares) of $^{22}$Ne/$^{20}$Ne matches the observed one (see text). For the set up adopted here we find we find $\upsilon_{min}$=1900 km/s for HMM models and $\upsilon_{min}$=2400 km/s for CL06 models.

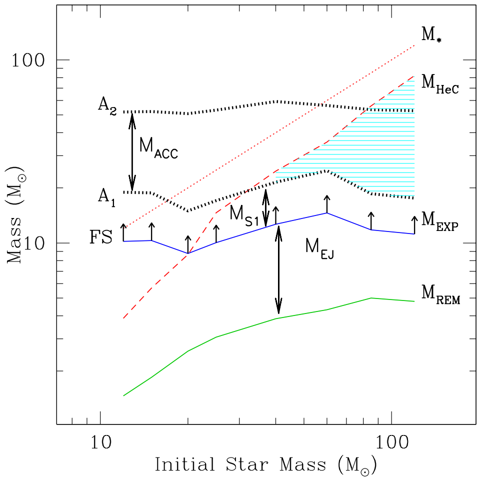


**Fig. 3.** Graphical presentation of the results discussed in Sec. 2. Particle acceleration starts at the beginning of the ST phase, located at mass coordinate $A_1$=$M_{Exp}$+ $M_{Ej}$, i.e. when the forward shock (FS, *arrows*), launched at $M_{Exp}$, has swept up a mass $M_{S1}$=$M_{Ej}$. Acceleration stops at mass coordinate $A_2$, corresponding in the case dicussed here to a shock velocity of 1900 km/s. The mass sampled by the FS between those two regions is $M_{Acc}$=$A_2$-$A_1$. For rotating stars with mass $M$ >30 $M_\odot$, an increasing part of $M_{Acc}$ includes nuclearly processed material (*shaded aerea*), while for rotating stars with $M$ <18 $M_\odot$, $M_{ACcc}$ contains only material of ISM (=solar) somposition.

solar units and $m_{22}(M_*)$ and $m_{20}(M_*)$ are swept up masses for star of mass $M_*$ and shock velocity ($\upsilon > \upsilon_{min}$).

The results of the procedure appear in Fig. 2 for a few selected abundance ratios and for the models of both HMM05 (*solid curves*) and CL06 (*dotted curves*). In all panels, the upper (*thin*) curves correspond to the composition accelerated at the beginning of the ST phase (maximal possible deviations from solar composition). It can be seen that stars with mass <22 $M_\odot$ (for HMM05) and 32 $M_\odot$ (for CL06) display no He-burning products in their accelerated particles. N is overabundant in lower stellar masses, due to the 1st dredge-up.

The lower (*thick*) curves in all panels of Fig. 2 correspond to composition accelerated *up to the end of the acceleration period* which is assumed to occur for a shock velocity $\upsilon_{min}$.

The corresponding IMF-averaged quantities (between 10 and 120 $M_\odot$) are displayed on the right of the curves: their uppermost point corresponds to the beginning of the ST phase and the lower one (also indicated with a *filled square*) to the end of the acceleration period, i.e. to $\upsilon_{min}$. The value of $\upsilon_{min}$ is found to be $\sim$ 1900 km/s for the HMM05 models with rotation and ~20% higher (2400 km/s) for the CL06 models without rotation. The reason for that difference is, of course the fact that rotating models have larger processed layers, requiring more dilution with circumstellar material.

The material of Sec. 2 is summarized in Fig.3 for the rotating models of HMM05. The forward shock, launched at mass coordinate $M_{Exp}$, sweeps up a mass $M_{S1} \sim M_{Exp}$ and then starts accelerating particles, at mass coordinate $A_1$=$M_{Exp}$+$M_{S1}$, up to point $A_2$ (where its velocity becomes $\upsilon_{min}$). For rotating stars with $M$ <15 $M_\odot$, $A_1$ lies beyond the stellar surface and only ISM is accelerated. In stars with 15<$M_*/M_\odot$<25, $A_1$ lies beyond the processed/mixed interior $M_{HeC}$ and the forward shock accelerates first envelope and then ISM material. For stars above 35 $M_\odot$, the shock first accelerates processed material (hatched aerea), then the - $^{22}$Ne normal - envelope and then ISM. Finally, for stars with M>70 $M_\odot$, particle acceleration ends when the shock is still within the massive stellar envelope.

As shown in Prantzos (2011), assuming that the spectrum of accelerated particles escaping the SN is a power law in momentum, one may find the efficiency with which particles are accelerated from the shocked circumstellar medium. For rotating stars it is found to be in the range 3-6 $10^{-6}$ i.e. a few particles out of a million encountered ones are accelerated by the forward shock to GCR energies. In the case of non-rotating stars, the energetics is the same, but the swept-up mass is smaller (by a factor of two, on average, in order to get the observed $^{22}$Ne/$^{20}$Ne ratio) and the corresponding efficiency is $W$ ~$10^{-5}$. These estimates constitute only a gross average, since the efficiency of particle acceleration may depend (among other things) on the density of the circumstellar medium or the shock velocity (through a smoothly varying function $f(\upsilon_S)$ instead of the Heaviside function $f(\upsilon_S > \upsilon_{min})$=1 and $f(\upsilon_S < \upsilon_{min})$=0 considered here). As approximate as they may be these results, obtained through the constrain of the observed GCR source $^{22}$Ne/$^{20}$Ne ratio, may help to improve our understanding of particle acceleration in SN remnants.

## References

Binns W. R., et al., 2005, ApJ, 634, 351
Binns W. R., et al., 2008, NewAR, 52, 427
Caprioli D., 2011, `arXiv:1103.4798`
Hirschi R., Meynet G., Maeder A., 2005, A&A, 433, 1013
Limongi M., Chieffi A., 2006, ApJ, 647, 483
Prantzos N., 2011, A&A, in press
Ptuskin V. S., Zirakashvili V., 2005, A&A, 429, 755